Origin of temperature-induced luminescence peak shifts from semipolar (11$\bar{2}$2) $In_xGa_{1-x}N$ quantum wells

Takuya Ozaki,* Mitsuru Funato, and Yoichi Kawakami†
Department of Electronic Science and Engineering, Kyoto University, Kyoto 615-8510, Japan
(Received 29 March 2017; revised manuscript received 16 August 2017; published 18 September 2017)

Observed temperature-induced peak shifts in photoluminescence (PL) originating from $In_xGa_{1-x}N$ single quantum wells grown on semipolar (11$\bar{2}$2) GaN bulk substrates are discussed in terms of a numerical exciton hopping model based on the Monte Carlo method. The experimentally observed PL peak shifts cannot be reproduced by conventional simulation models developed for the polar (0001) plane, where the recombination lifetime is assumed to be temperature independent, and blue-shifts in PL signal are found to be induced by exciton thermal repopulation. Therefore, we incorporate temperature-dependent radiative and nonradiative recombination processes into the model, in which temperature-induced reductions in recombination lifetimes effectively limit the exciton motion. This model is found to be a much better fit for the data, indicating that, in addition to the thermal repopulation process, the reduction of lifetime with increasing temperature can also contribute to the PL blue-shift because shortened lifetimes suppress the exciton motion and therefore produce smaller Stokes shifts. We propose that the dominant factor responsible for the PL blue-shifts depends on the degree of potential fluctuation.

DOI: 10.1103/PhysRevB.96.125305

I. INTRODUCTION

Ternary and quaternary alloys of III-nitride semiconductors are key materials for many device applications, such as light-emitting diodes [1,2], laser diodes [3,4], and solar cells [5] in the infrared-to-ultraviolet spectral range. Their optical and electrical properties are inevitably influenced by random fluctuations in alloy composition, the widths of the quantum wells (QWs), and strain, and these effects have been studied extensively. One remarkable feature is that the emission is generated via radiative recombination of excitons localized in the lower-energy states in the potential fluctuation [6,7]. The exciton localization induces a unique temperature dependence of the luminescence peak: S-shaped peak shifts have been observed for polar $In_xGa_{1-x}N$ (Refs. [8–11]) and $Al_xGa_{1-x}N$ (Refs. [12–14]) alloys, and are explained as follows: a temperature increase in the low-temperature range causes exciton transfer to lower-energy states (red-shift) because the excitons localized in the disordered potential gain thermal energy. A further temperature increase repopulates excitons to higher-energy states (blue-shift) according to a Bose-Einstein distribution. At sufficiently high temperatures, the peak energy shifts toward lower energy (red-shift) due to the temperature dependence of the band-gap energy.

Experimentally observed temperature dependencies of photoluminescence (PL) peak energies and their full widths at half-maximum (FWHMs) have been analyzed by Monte Carlo simulations of phonon-assisted exciton hopping in inhomogeneously distributed localization states [10,13,15–21]. This method has been used widely, not only for III-nitride semiconductors [10,13,17], but also for other III-V (Refs. [18,19]) and II-VI (Refs. [20,21]) species. However, previous reports have assumed a constant recombination probability irrespective of temperature and energy, which may significantly affect the degree to which they can reproduce the experimental results (examples are shown in Sec. IV.) In fact, Langer *et al.* [22] have recently reported that the energy dependence of radiative lifetimes due to polarization fields can also produce the S-shaped PL shift in polar $In_xGa_{1-x}N$ QWs.

Here, we demonstrate the impact of the temperature dependence of exciton recombination lifetimes on the PL peak energies and FWHMs originating from $In_xGa_{1-x}N$ QWs. Exciton lifetimes are generally determined by radiative and nonradiative lifetimes, and are thus quite sensitive to temperature. With increasing temperature, the PL decay time tends to decrease due to the increased contribution of a nonradiative recombination component [23]. In addition, the reduced exciton lifetime hinders the exciton hopping motion and reduces the Stokes shift, which may also result in the blue-shift. Although Cho *et al.* [9] have suggested this mechanism for the experimentally observed temperature dependence of PL peaks from (0001) $In_xGa_{1-x}N$ QWs, evidence based on quantitative discussion has yet to be produced.

The samples used in this study are semipolar (11$\bar{2}$2) $In_xGa_{1-x}N$ single QWs (SQWs) with various In compositions and QW widths. The PL peak shifts from these SQWs exhibit various temperature-dependent features, such as monotonous red-shifts or S-shaped shifts. Interestingly, these experimental results cannot be reproduced by the exciton hopping model without including a consideration of the temperature-induced change in the exciton lifetimes. Therefore, it may be concluded that both the thermal repopulation process and the temperature dependence of the recombination lifetime play key roles in determining the PL temperature dependencies; additionally, we demonstrate that the dominant factor causing the PL peak shifts varies, depending on the degrees of inhomogeneity and exciton lifetime variation.

This paper is composed of seven sections. In Sec. II, the widely accepted theoretical descriptions of luminescence properties in disordered materials are briefly reviewed. In Sec. III, details of the sample structures and experimental procedures are presented. In Sec. IV, the experimental results

*Present address: Nichia Corp., Anan, Tokushima 774-8601, Japan.
†kawakami@kuee.kyoto-u.ac.jp

for polar (0001) and semipolar (11$\bar{2}$2) $In_xGa_{1-x}N$/GaN SQWs are compared with theoretical predictions described in Sec. II. It is demonstrated that the simulations do not necessarily agree well with the experiments and, thus, another model that considers temperature-induced lifetime variations is developed in Sec. V, which is shown to achieve quantitative agreements with all of the experimental results. Furthermore, the decisive factors of the temperature-induced peak energy variation are discussed in Sec. VI; finally, Sec. VII summarizes our study.

II. THEORETICAL CALCULATIONS

This section briefly presents theoretical treatments for the temperature dependence of PL peak energies and FWHMs, based on the exciton hopping model. A disordered potential induced by fluctuations in, for example, alloy composition and QW width gives rise to a low-energy tail in the density of states, which affects the recombination dynamics of electrons and holes. For GaN-based III-nitride semiconductors, excitons, which are quasiparticles composed of electron-hole pairs, must be considered because the exciton binding energy is larger than the thermal energy, even at room temperature (RT) [24]. In this situation, an exciton can be treated as a single particle moving in an effective disordered potential. Because excitons coupled with the phonon system can move both spatially and energetically [25], the resulting PL spectra are located at a lower energy than the absorption spectra, which is referred to as the Stokes shift.

As a result of temperature-induced variation of the exciton motion in an inhomogeneous potential distribution, the PL peak energies and FWHMs vary anomalously with temperature. It has often been reported that such behaviors can be quantitatively analyzed by a two-dimensional (2D) Monte Carlo simulation of the hopping process [15,16], as described below.

Initially, recombination sites with a sheet density N and a random distribution of potential energies are prepared. The potential energy distribution [$D(E)$] is assumed to be expressed by a Gaussian function

$$D(E) \propto \exp\left[-\frac{(E-E_0)^2}{2\sigma^2}\right], \tag{1}$$

where E_0 is the mean potential energy and σ is the standard deviation describing the energy scale of the potential fluctuation. Photogenerated excitons with excess energy are assumed to instantly relax to the band edge and evenly occupy the recombination sites described by Eq. (1).

The phonon-assisted hopping rate between two energy states ($\nu_{i\to j}$) is described by the Miller-Abrahams tunneling rate [26]

$$\nu_{i\to j} = \nu_0 \exp\left(-\frac{2r_{ij}}{\alpha} - \frac{E_j - E_i + |E_j - E_i|}{2k_BT}\right), \tag{2}$$

where E_i and E_j are the energies of sites i and j, respectively, r_{ij} is the distance between the two sites, α is the decay length of the localized exciton center-of-mass wave function, ν_0 is the attempt-to-escape frequency, and k_B is the Boltzmann constant. For each generated exciton, the hopping process is terminated by recombination with a rate τ_0^{-1}. Here, τ_0 is usually assumed to be independent of temperature and energy (as described later in Sec. IV, this assumption is not always valid.) The emission spectrum $S_0(E)$ is produced by counting the number of excitons as a function of the energy at which recombination takes place. The simulation results depend on the spatial and temporal parameters represented by $N\alpha^2$ and $\tau_0\nu_0$, respectively.

To see the influence of potential fluctuation on the emission properties, emission spectra were simulated for some σ values. Figure 1 presents (a) FWHMs and (b) Stokes shifts estimated from the simulated spectra as functions of temperature. The FWHM [Fig. 1(a)] shows an initial increase and subsequent saturation with temperature. Although exciton thermal repopulation can occur at any temperature, the initial increase in the FWHMs suggests that the thermal energy is not sufficient for excitons to reach the higher-energy states within the potential energy distribution, while the subsequent saturation suggests that excitons can reach nearly all of the states, resulting in peaks with FWHMs equal to those of the potential energy distribution ($=2\sqrt{2\ln 2}\sigma$); note that larger σ values heighten the transition temperature between these two conditions. As for the Stokes shift, as seen in Fig. 1(b), the observed initial increase (i.e., red-shift in luminescence) indicates that, in the low-temperature regime, exciton repopulation occurs

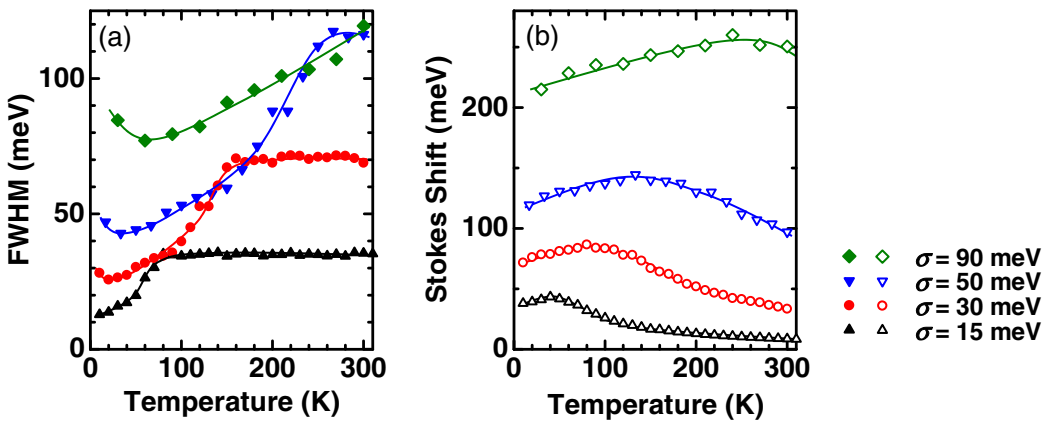

FIG. 1. Examples of simulations for (a) PL FWHMs and (b) Stokes shifts as functions of temperature. The selected σ values are 15 meV (triangles), 30 meV (circles), 50 meV (inverse triangles), and 90 meV (diamonds); other parameters are $\tau_0\nu_0 = 1 \times 10^5$ and $N\alpha^2 = 1$. Solid lines are used as a visual guide.

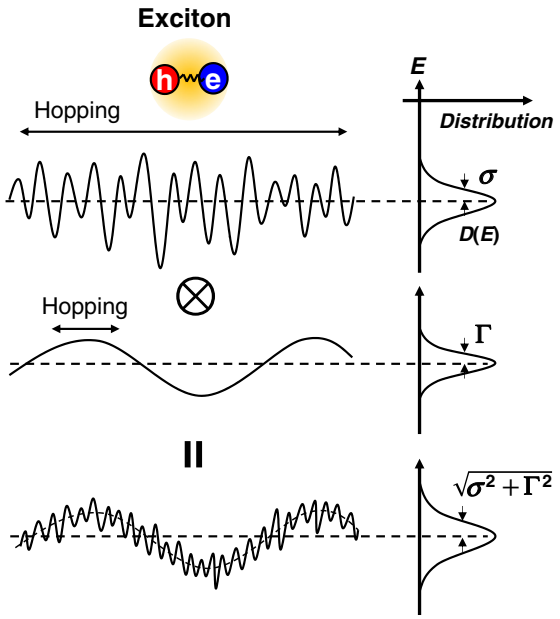

FIG. 2. Schematic diagram of double-scaled potential fluctuations. The regions in which excitons are mobile are characterized by the potential energy distribution $D(E)$ with σ. This short-range inhomogeneity superimposes on a long-range inhomogeneity with Γ.

predominantly toward lower energies, while above a certain temperature, the Stokes shift decreases (i.e., blue-shift in luminescence) due to the thermal repopulation of excitons. Again, it is noteworthy that larger σ values increase the temperature at which the maximum Stokes shift is observed because excitons need larger thermal energy to overcome the higher potential barrier caused by the larger values of σ.

To quantitatively fit to the experimentally observed FWHMs, an additional long-range inhomogeneous-broadening parameter Γ should be introduced [13]. Figure 2 presents schematic images of fluctuations in the double-scaled potential profiles. It is assumed that the exciton hopping motion is restricted within a region characterized by the potential energy distribution with σ, and that the spatial scale of Γ is sufficiently larger than that of the exciton motion. In fact, the use of both scanning near-field optical microscopy (SNOM) and conventional optical microscopy has revealed the coexistence of $\sim\mu$m scale and $\sim$100 nm scale fluctuations in QWs of $In_xGa_{1-x}N$ (Refs. [11,27–30]) and $Al_xGa_{1-x}N$ [31], and that excitons are mobile within the smaller-scale fluctuations. The resultant spectral shape $S(E)$ can be written as

$$S(E) = \int S_0(E')G(\Gamma, E - E')dE', \tag{3}$$

where $G(\Gamma, E)$ is a Gaussian function with deviation Γ. The FWHM values estimated from Eq. (3) as a function of temperature $[\Gamma_{inh}(T)]$ can adequately reproduce the experimental FWHMs in a relatively low-temperature range where the FWHM increases with temperature. However, with further increases in temperature, the experimental FWHM values become larger than those predicted theoretically because interactions with phonons become dominant. Thus, the total FWHM as a function of temperature $\Gamma_{total}(T)$ can be written as

$$\Gamma_{total}(T) = \Gamma_{inh}(T) + \Gamma_{ph}(T) = \Gamma_{inh}(T) + \beta T + \frac{\gamma}{\exp(\hbar\omega_{LO}/k_BT) - 1}, \tag{4}$$

where $\Gamma_{ph}(T)$ is an FWHM component determined by interaction with phonons, and β and γ represent the exciton/carrier coupling strengths with acoustic and longitudinal optical (LO) phonons, respectively [32]. The contributions from acoustic phonons (βT) are generally observable at low temperatures, but tend to be obscured by the broadening described in Eq. (3). For LO phonons, we assume that the LO phonon energy ($\hbar\omega_{LO}$) of $In_xGa_{1-x}N$ can be interpolated linearly from the related materials GaN (91.3 meV) (Ref. [33]) and InN (73.5 meV) (Ref. [34]). In our analyses of luminescence from polar (0001) SQWs, we used $\beta = 0.013$ meV/K and $\gamma = 0.47$ eV, as reported for (0001) GaN (Ref. [35]) because there are no reliable data for InN. For the semipolar $(11\bar{2}2)$ SQWs, there have been no data reported for these parameters, and therefore values of $\beta = 0.035$ meV/K and $\gamma = 0.75$ eV, which have been reported for a nonpolar $In_xGa_{1-x}N$ SQW [30], were used, independent of the samples. These values were able to suitably reproduce the experimentally obtained temperature dependence of FWHMs for both polar and semipolar QWs. It should be noted that the strength of an electron-phonon interaction depends on properties of the QWs such as built-in potentials. The larger β and γ values for the semipolar QWs (as well as nonpolar QWs) imply that electron-phonon interactions are enhanced in the semipolar QWs, most likely due to the much larger inhomogeneities shown below. The homogeneous broadening was neglected because its contribution to the FWHM is considerably smaller in comparison with inhomogeneous broadening. The parameter $\Gamma_{total}(T)$ is applicable for fitting over the whole temperature range.

Figure 3(a) shows an example of FWHMs calculated as functions of temperature. The broadening parameter σ was 30 meV, and the $\Gamma_{inh}(T)$ ($\Gamma = 0$ meV), represented by the open squares, corresponds to the FWHM in Fig. 1(a). The additional broadening due to long-range inhomogeneity, Γ, leads to the offset in the temperature behavior, as shown by $\Gamma_{inh}(T)$ ($\Gamma = 20$ meV) (filled squares). Further consideration of the broadening due to phonon interaction can produce the W-shaped trend in the FWHM values, as has been reported in various studies [10,17]: this is shown by $\Gamma_{total}(T)$ (half-filled squares).

In addition to the FWHM, the simulation predicts the Stokes shift ΔE_{Stokes}, which is the difference between the PL peak energy $E_{PL}(T)$ and the mean potential energy $E_0(T)$:

$$\Delta E_{Stokes}(T) = E_0(T) - E_{PL}(T). \tag{5}$$

The temperature dependence of the band-gap energy is assumed to be described by a Bose-Einstein–type expression [36]. This produces the expression

$$E_0(T) = E_0(0\text{ K}) - \frac{2a_B}{\exp(\Theta/T) - 1}, \tag{6}$$

where a_B represents the average strength of the exciton-phonon interaction and Θ corresponds to the average phonon temperature. Because the exciton-phonon interaction may

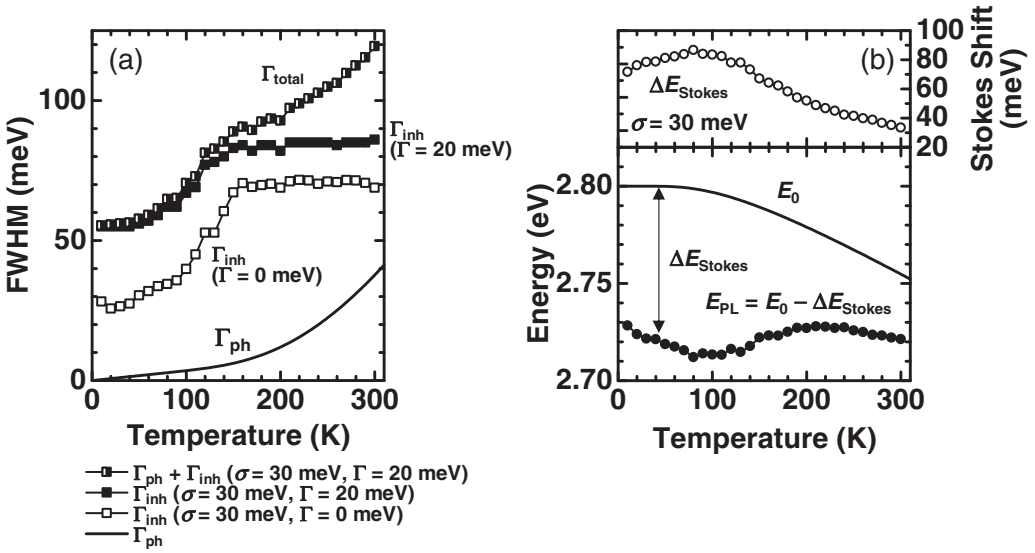

FIG. 3. Example simulation results for $\sigma = 30$ meV. (a) FWHMs as functions of temperature. The solid line represents Γ_{ph}. The following plots are shown: Γ_{inh} with $\Gamma = 0$ meV (open squares), Γ_{inh} with $\Gamma = 20$ meV (filled squares), and Γ_{total} (half-filled squares). (b) ΔE_{Stokes}, E_0, and E_{PL} as functions of temperature. In the calculation, values of $\tau_0\nu_0 = 1 \times 10^5$, $N\alpha^2 = 1$, and $E_0(0\,\mathrm{K}) = 2.800$ eV were used.

depend on the properties of the QWs and the potential fluctuation through the variation in exciton confinement, in this study, a_B and Θ values are treated as variables in the ranges of 35–50 meV and 350–450 K, respectively, which lie within the variation ranges for the reported values from GaN (Refs. [37–39]) and InN (Ref. [40]).

Figure 3(b) shows an example of a simulated Stokes shift, $\Delta E_{Stokes}(T)$, and PL peak energy [$= E_0(T) - \Delta E_{Stokes}(T)$] as functions of temperature. The S shape of the PL peak energy, which is frequently observed in experiment, is well reproduced, as shown in the lower panel of Fig. 3(b). In the fitting procedure below, the fitting parameters σ, Γ, $\tau_0\nu_0$, $N\alpha^2$, and $E_0(0\,\mathrm{K})$ were used.

III. EXPERIMENTAL PROCEDURES

The samples discussed in this study were grown by metal-organic vapor phase epitaxy. The substrates were semipolar $(11\bar{2}2)$ GaN sliced from [0001]-oriented GaN crystals grown by hydride vapor phase epitaxy. Prior to film deposition, the substrate surfaces were chemically and mechanically polished. Initially, 2-μm-thick, unintentionally doped homoepitaxial GaN layers were grown on the substrates. Then, coherent $In_xGa_{1-x}N$/GaN SQWs were grown; details of the growth conditions are described in Ref. [41].

The structural parameters of the SQW samples were evaluated by x-ray diffraction (XRD) radial scans around the $(11\bar{2}2)$ symmetric plane, and are summarized in Table I. To determine the In compositions of the coherently strained $(11\bar{2}2)$ $In_xGa_{1-x}N$ layers, we used a strain model proposed in Ref. [42]. Samples A and B were violet and green emitters with estimated In compositions of ~14% and ~24%, and well widths of 4.0 and 2.6 nm, respectively, while samples C to E had similar In compositions of ~20%, but different well widths in the range of 2.0–5.1 nm.

Temperature-dependent PL measurements were performed using a closed-cycle cryostat to vary the temperatures from 13 to 300 K. The QW layers were selectively excited using the second harmonic wave of a Ti:sapphire pulse laser with an emission wavelength of 400 nm. The pulse width and repetition rate were 1.5 ps and 80 MHz, respectively, and the excitation energy density per pulse was 1.6 μJ/cm^2, which corresponds to an estimated initial carrier density of 1.4×10^{17} cm^{-3}. The emissions from the surface normal were projected into a 25-cm spectrometer and recorded by a charge-coupled device detector.

PL excitation (PLE) measurements were also performed at 13 and 100 K. Quasimonochromatic light with a spectral width of 1 nm was obtained from a Xe lamp dispersed with a 50-cm monochromator. The detection setup was the same as that for PL. The PLE signals were produced at the emission peak energies.

To evaluate exciton recombination lifetimes, temperature-dependent time-resolved PL (TRPL) measurements were performed at temperatures between 5 and 300 K. The excitation conditions were the same as those for PL, except that different pulse repetition rates (depending on the particular sample), selected from 0.8, 4, or 80 MHz using an acousto-optic modulator, were used to avoid multiexcitation. The TRPL signals were detected in the direction normal to the surface, using a streak camera in conjunction with a 30-cm monochromator.

TABLE I. In compositions x and well widths L_w of the semipolar $(11\bar{2}2)$ $In_xGa_{1-x}N$/GaN SQWs estimated from XRD data. The GaN cap layers were ~10 nm thick.

Samples	x	L_w (nm)
A	0.14	4.0
B	0.24	2.6
C	0.22	2.0
D	0.19	3.8
E	0.21	5.1

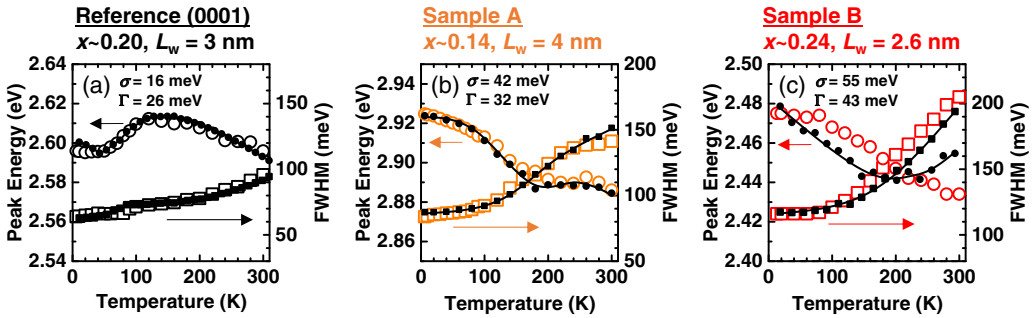

FIG. 4. PL peak energies (circles) and FWHMs (squares) of (a) a typical blue-emitting (0001) $In_xGa_{1-x}N$/GaN SQW, (b) sample A ($x = 0.14$, $L_w = 4.0$ nm), and (c) sample B ($x = 0.24$, $L_w = 2.6$ nm) as functions of temperature. The open and filled symbols depict the experimental and simulated data, respectively. In the simulation, the exciton lifetime was assumed to be constant, similar to the conventional method. The solid lines are included as a visual guide.

The spectral resolution of the detector for all the PL-related measurements was less than 0.2 nm, which is much narrower than the PL linewidths.

IV. ANALYSES WITH THE CONVENTIONAL MODEL

The shapes of the PL spectra are slightly asymmetric and possess low-energy tails, most likely due to merging of LO phonon replicas. The PL peak energies and FWHMs of the direct transition components (zero phonon lines) were determined by fitting multiple Gaussian functions separated by the LO phonon energy. The FWHM of each Gaussian component was assumed to be the same. At higher temperatures, the relative intensities of the side-band components to the main peak became stronger, which supported the assignment of these components to the LO phonon replicas.

Figure 4 shows temperature-dependent PL peak energies and FWHMs from (a) a reference polar (0001) SQW, and (b) sample A [$x = 0.14$, well width (L_w) = 4.0 nm] and (c) sample B ($x = 0.24$, $L_w = 2.6$ nm) semipolar ($11\bar{2}2$) SQWs. The polar sample is a typical blue emitter with a well width of ~3 nm grown on sapphire. The S-shaped peak shift was clearly observed in the polar sample, and was slightly visible in sample A. On the other hand, sample B showed a monotonous red-shift up to RT, rather than S-shaped behavior.

To explain the experimental results, we performed simulations based on the exciton hopping model described in Sec. II. Initially, the temperature dependence of FWHMs was fitted, and then the PL peak energies were simply simulated with the fitted parameters, as per the same procedure in Ref. [10]. Here, the fitting parameters were σ, Γ, $\tau_0\nu_0$, $N\alpha^2$, and $E_0(0\,\mathrm{K})$, as described in Sec. II.

Figure 4 compares the experimental and simulated results for both the FWHMs and the PL peak energies; the fitted parameters are listed in Table II. Note that the lifetime is assumed to be temperature independent. Even with this conventional procedure, the experimental results for the polar sample and sample A were quantitatively reproduced. (The significant digit for each parameter suggests an error of the estimate.) However, for sample B, the simulated peak energy did not show a monotonous red-shift as observed by experiment, but instead yielded a blue-shift at temperatures higher than ~220 K. Instead of the Gaussian distribution [Eq. (1)], an exponential-type distribution [15,16] was also examined, but the fitting was not successful.

In addition, the PLE measurement for sample B revealed that the mean potential energy E_0 at 13 K was 2.713 ± 0.015 eV, as shown in Fig. 5. Here, E_0 was extracted by fitting the Urbach tail relation [43]

$$\alpha(E) = \frac{\alpha_0}{1 + \exp[(E_0 - E)/\Delta E]} \tag{7}$$

to the PLE spectrum. In Eq. (7), α_0 is the intrinsic absorption coefficient and ΔE is a broadening parameter. E_0 estimated from PLE (2.713 eV) was found to be much larger than that from the simulation (2.610 eV); although we ran a second exciton hopping simulation with a constant $E_0(0\,\mathrm{K}) = 2.713$ eV derived from PLE, we were not able to achieve better reproducibility, as shown in Fig. 6. The fitting parameters were reduced to σ, Γ, $\tau_0\nu_0$, and $N\alpha^2$, and the obtained parameters were $\sigma = 103$ meV, $\Gamma = 22$ meV, $\tau_0\nu_0 = 1 \times 10^4$, and $N\alpha^2 = 1$.

We consider that the disagreement between the experiment and simulation, as shown in Figs. 4(c) and 6, was caused by the assumption that exciton lifetimes are temperature independent. The recombination lifetime τ is determined by radiative and nonradiative recombination lifetimes (τ_{rad} and τ_{nonrad}, respectively) via the relation $1/\tau = 1/\tau_{rad} + 1/\tau_{nonrad}$. Theoretically, τ_{rad} in a 2D system like QWs should have a linear temperature dependence [44]; on the other hand, τ_{nonrad} is determined by carrier capture to nonradiative recombination centers and expressed as $\tau_{nonrad} = 1/v_{th}\sigma_c N_{nr} \propto T^{-0.5}\exp(E_a/k_BT)$ [45]. Here, v_{th} is the thermal velocity, σ_c is the capture cross section, N_{nr} is the density of nonradiative recombination centers, and E_a is their activation energy. Thus, τ_{rad}, τ_{nonrad}, and the subsequent values of τ strongly depend on temperature. Because the exciton motion is determined by

TABLE II. Parameter sets used in the conventional simulation method.

Samples	σ (meV)	Γ (meV)	$\tau_0\nu_0$	$N\alpha^2$	$E_0(0\,\mathrm{K})$ (eV)
(0001) SQW	16	26	1×10^5	1	2.641
A	42	32	3×10^3	1	3.018
B	55	43	1×10^5	1	2.610

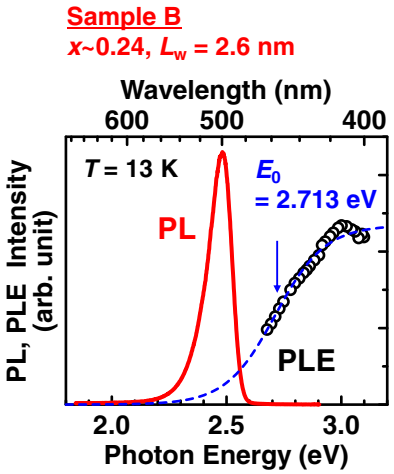

FIG. 5. PL and PLE spectra acquired at 13 K from sample B ($x = 0.24$, $L_w = 2.6$ nm). The dashed line is the fitted curve calculated with Eq. (7). The estimated mean potential energy is 2.713 ± 0.015 eV.

the competition between hopping transfer and recombination, temperature-induced lifetime variations can affect the exciton population in a disordered potential.

V. DEVELOPING A MODEL WITH CONSIDERATION OF TEMPERATURE-DEPENDENT LIFETIMES

To include the temperature-dependent exciton lifetime into the hopping model, TRPL spectroscopy was performed. Figure 7(a) presents PL decay curves monitored representatively at the peak energies of sample B at temperatures of 5 and 300 K. The PL decay exhibited non-single-exponential behavior, which is typically observed in disordered systems, and is attributed to spatially isolated recombination processes [46,47]. By fitting the convolution of the laser profile and a single exponential function to the initial decays, the PL decay time was evaluated. Figure 7(b) shows the time-integrated PL (TIPL) spectrum and the PL decay times as functions of the photon energy. The energy

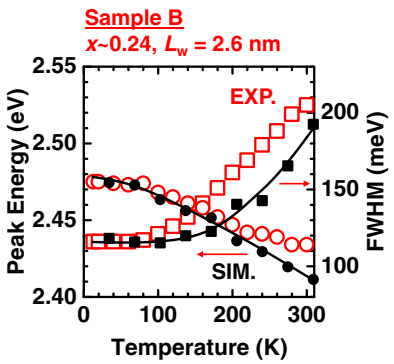

FIG. 6. Refitting of the PL temperature dependencies of sample B ($x = 0.24$, $L_w = 2.6$ nm) using $E_0(0\,\mathrm{K}) = 2.713$ eV derived from PLE. Open and filled symbols represent the experimental and fitting results, respectively. The obtained parameters are $\sigma = 103$ meV, $\Gamma = 22$ meV, $\tau_0\nu_0 = 1 \times 10^4$, and $N\alpha^2 = 1$. The solid lines are included as a visual guide.

dependence of the decay time has a plateau around the PL peak, and is quite typical for weakly localized excitons in a disordered potential [48]; Ref. [48] has suggested that, theoretically, the faster decay time in the higher-energy regime is due to the transfer of weakly localized excitons from higher- to lower-energy states, whereas the constant decay time in the lower-energy regime corresponds to the recombination lifetime. In this study, the estimated recombination lifetime was 0.65 ns: because the PL lifetime at the peak energy (0.60 ns) is close to 0.65 ns, it is taken as being representative of the PL lifetime in the following discussion. Here, it should be noted that the effect of the polarization field on the energy dependence of the decay time [22] was ignored. This is because the inhomogeneous broadening in our samples is mainly due to In compositional fluctuations, as mentioned below, and our calculations of the square overlaps of electron and hole wave functions for $In_xGa_{1-x}N$ QWs with various In compositions cannot reproduce the experimental trend shown in Fig. 7(b). Figure 7(c) plots the PL lifetime τ as a function of temperature. The radiative (τ_{rad}) and nonradiative (τ_{nonrad}) recombination lifetimes were extracted using the method described in Ref. [49], showing that, on increasing the temperature from 5 to 300 K, the PL lifetime decreased to one-fifth of its original value due to contributions from a nonradiative process.

The experimentally determined PL lifetime $\tau(T)$ was used in the simulation. Figure 8(a) compares the experimental and simulation data for the PL peak energies and FWHM of sample B, using the model developed in this study. The fitted parameters were $\sigma = 110$ meV, $\Gamma = 0$ meV, $\nu_0 = 5 \times 10^{12}\,\mathrm{s}^{-1}$, $N\alpha^2 = 1$, and $E_0(0\,\mathrm{K}) = 2.710$ eV. The quantitative agreement between the two sets of data was found to drastically improve for both the PL peak energies and FWHMs, compared with the conventional analyses in Figs. 4(c) and 6. Additionally, in comparison with a conventional model with similar σ values (Fig. 6), the modified model was found to yield higher emission energies and wider FWHMs, particularly at elevated temperatures. This is due to the reduced lifetimes at high temperatures, which prevents excitons from hopping toward lower-energy states, thereby realizing the energetically broad distributions of excitons within the potential fluctuation.

Considering the simulated Stokes shift and the experimental PL peak energy, the temperature dependence of the mean potential energy was constructed with $E_0(T) = E_{PL}(T) + \Delta E_{Stokes}(T)$, and plotted in Fig. 8(b) (inverse triangles). Then, Eq. (6) was fitted to the evaluated $E_0(T)$. As shown by the solid line in Fig. 8(b), a reasonably good fit was achieved with the parameters $E_0(0\,\mathrm{K}) = 2.710$ eV, $a_B = 50$ meV, and $\Theta = 350$ K. It is noteworthy that the $E_0(0\,\mathrm{K})$ values estimated using the hopping simulation and Eq. (6) lie in complete agreement. In addition, Fig. 8(b) plots the E_0 values evaluated from the PLE measurements at 13 and 100 K (diamond symbols), which were found to agree quite well with the $E_0(T)$ values derived from the simulations and PL. As such, we demonstrate that three different ways can be used to adequately reproduce the temperature dependence of $E_0(T)$, which confirms that the modified method developed in this study can reliably predict the temperature behavior of the luminescence properties of $In_xGa_{1-x}N$ QWs.

To further demonstrate the robustness of our model, we applied it to three other $(11\bar{2}2)$ $In_xGa_{1-x}N$/GaN SQW samples.

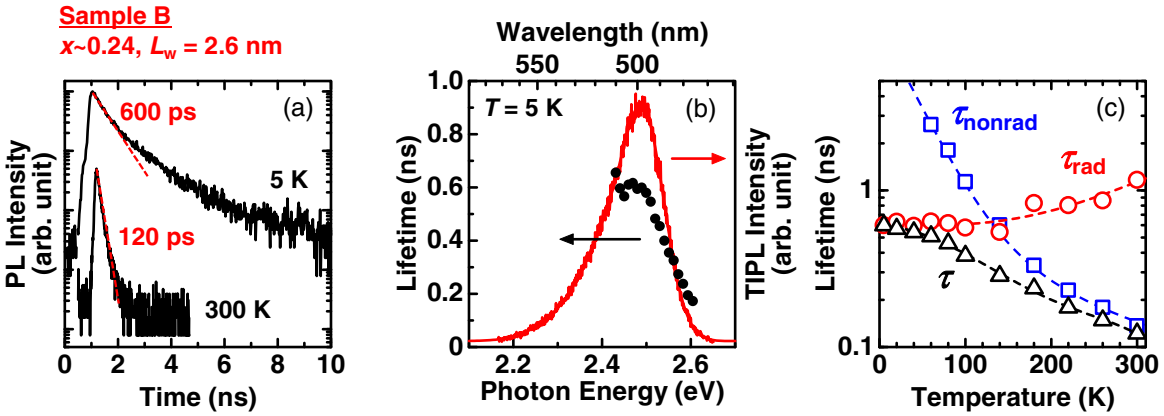

FIG. 7. (a) PL decay curves at the peak energy of sample B ($x = 0.24$, $L_w = 2.6$ nm) at 5 and 300 K. (b) TIPL spectrum and the initial decay time at 5 K as functions of photon energy. (c) PL initial decay time, and radiative and nonradiative recombination lifetimes as functions of temperature. Dashed lines are included as a visual guide.

These samples have almost the same In composition as sample B (~20%), but different QW widths. As demonstrated in the Supplemental Material [50], the energy dependencies of their PL lifetimes at low temperature are quite similar to that of sample B shown in Fig. 7(b). Therefore, the energy-dependent PL lifetimes seem not to be responsible for the variation of the temperature-induced PL peak shifts discussed below.

Figures 9(a)–9(c) present the temperature-dependent PL peak energies of samples C ($x = 0.22$, $L_w = 2.0$ nm), D ($x = 0.19$, $L_w = 3.8$ nm), and E ($x = 0.21$, $L_w = 5.1$ nm), respectively. (To avoid repeating similar discussions, the FWHMs are excluded from Fig. 9.) The PL spectra of the wider QW samples were located at lower energies, mainly because of the quantum confinement Stark effect (QCSE) caused by electric fields along the growth direction, although it is suppressed by growth on $(11\bar{2}2)$ planes. A comparison between the experimental and theoretical [51] red-shift of PL peak energies with increasing QW thickness can be used to deduce the internal electric fields, which were found to fall in the range 0.4–0.5 MV/cm (it is noted that the electric fields calculated for polar QWs with an In composition ~20% were found to be higher than 2 MV/cm.) The blue-shift of the PL peak with increasing temperature was observed to be more marked for samples with thicker QWs.

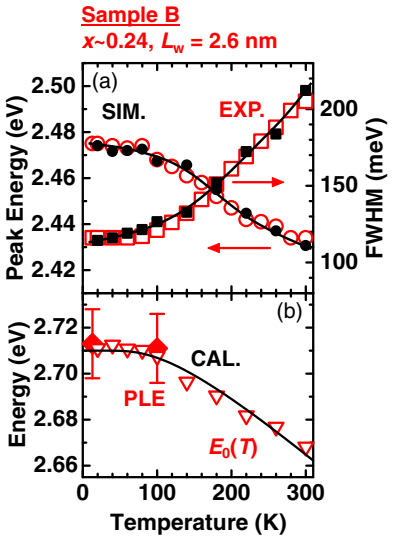

FIG. 8. (a) PL peak energies (circles) and FWHMs (squares) of sample B ($x = 0.24$, $L_w = 2.6$ nm) as functions of temperature. The open and filled symbols denote the experimental and simulated data sets, respectively. The simulation was performed with method developed in this study, in which temperature-dependent lifetimes estimated by TRPL are used. The fitted parameters are $\sigma = 110$ meV, $\Gamma = 0$ meV, $\nu_0 = 5 \times 10^{12}$ s^{-1}, $N\alpha^2 = 1$, and $E_0(0\,\mathrm{K}) = 2.710$ eV. The solid lines are included as a visual guide. (b) Temperature dependence of the mean potential energy constructed from the experimental PL peak energies and the simulated Stokes shift (inverse triangles). The solid line was calculated with Eq. (6). The exciton energies estimated from the PLE measurements at 13 and 100 K (diamonds) are also plotted.

First, the obtained results were analyzed using the conventional analytical method, which attributes the PL blue-shift solely to the thermal repopulation of localized excitons. Within this framework, it is widely accepted that the degree of the blue-shift in the relatively high-temperature range is characterized by σ, and can be expressed by following a simple band-filling model [8]

$$E_{\mathrm{peak}}(T) = E_0(T) - \frac{\sigma^2}{k_B T}, \tag{8}$$

where σ is the already defined standard deviation of the Gaussian distribution [Eq. (1)]. Fitting Eq. (8) to the blue-shifts in samples D and E [solid lines in Figs. 9(b) and 9(c), respectively] provided $\sigma = 17$ and 28 meV, respectively. Using these values, the peak shifts over the whole temperature range were simulated by the conventional hopping model, using constant τ values. (For sample C, the estimated σ from the hopping simulation was 85 meV.) Figure 9(a) shows that the simulation for sample C (thin QW) can reproduce the experimental peak shift over the whole temperature range. On the other hand, Fig. 9(c) provides calculated data for sample E (thicker QW), and shows a large discrepancy in the lower-temperature range. In addition, the PL FWHMs at low temperature were 101, 125, and 181 meV for samples C, D, and E, respectively (see Supplemental Material [50]), which are inconsistent with the estimated trend in σ values.

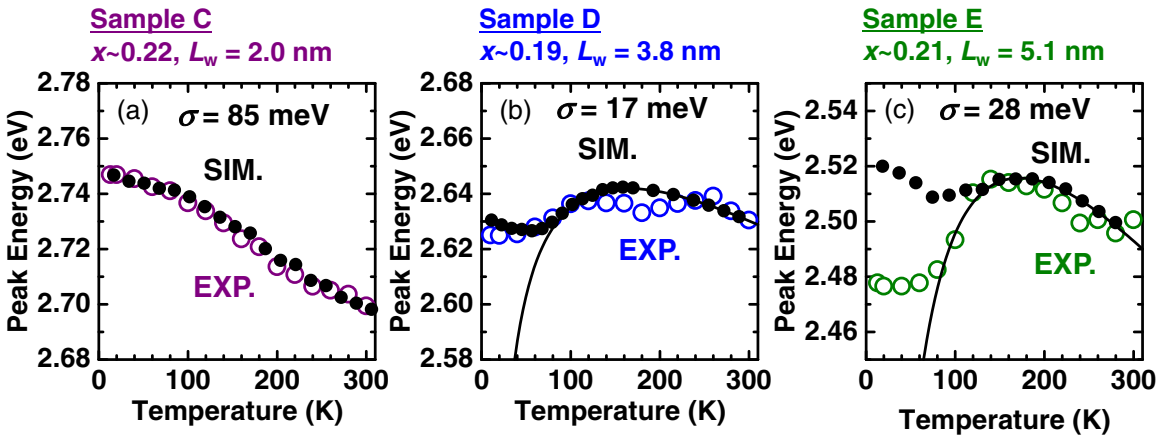

FIG. 9. Temperature-dependent PL peak energies of samples (a) C ($x = 0.22$, $L_w = 2.0$ nm), (b) D ($x = 0.19$, $L_w = 3.8$ nm), and (c) E ($x = 0.21$, $L_w = 5.1$ nm). Filled circles represent the simulation results obtained by the conventional method, using σ values of (a) 85 meV, (b) 17 meV, and (c) 28 meV. Solid curves are the fitting results obtained using Eq. (8).

The above analyses indicate that thermal re-population of excitons is not responsible for the observed S shape in the PL spectra of the $(11\bar{2}2)$ SQWs. Therefore, we decided to take into consideration the effect of declining exciton lifetime with increasing temperature. The lower figures in Fig. 10 show the PL recombination lifetimes of the three samples as functions of temperature: at low temperatures, the PL lifetimes are mainly determined by radiative processes as the nonradiative process is inactive [49]; as such, wider QWs show longer τ at low temperatures because the polarization field reduces the optical transition probability more significantly than in narrower QWs. Around RT, the nonradiative process starts to dominate the PL lifetime. This process is not affected by the well width; therefore, the nonradiative lifetimes of samples C to E were expected to be similar, as they were grown under identical conditions, with the exception of growth time. In fact, at RT, similar PL lifetimes were observed for all the samples. As a consequence, the PL lifetime variation is more significant for wider QWs, which is demonstrated in Fig. 10. It should be noted that sample E is much thicker than typical InGaN QWs, so that the variation of the PL lifetime due to the measurement temperature is more considerable. A similar well-width dependence of the temperature-induced PL lifetime variations has also been reported for (0001) InGaN QWs [52].

The upper panels in Fig. 10 represent the simulation results calculated using our model, taking into account the lifetime variations: these agree fairly well with the experimental data. Table III summarizes the derived parameters. The estimated σ values were 90, 110, and 140 meV for samples C, D, and E, respectively, which are consistent with the aforementioned low-temperature FWHM values. Generally, a compositional fluctuation causes a larger potential fluctuation in a wider

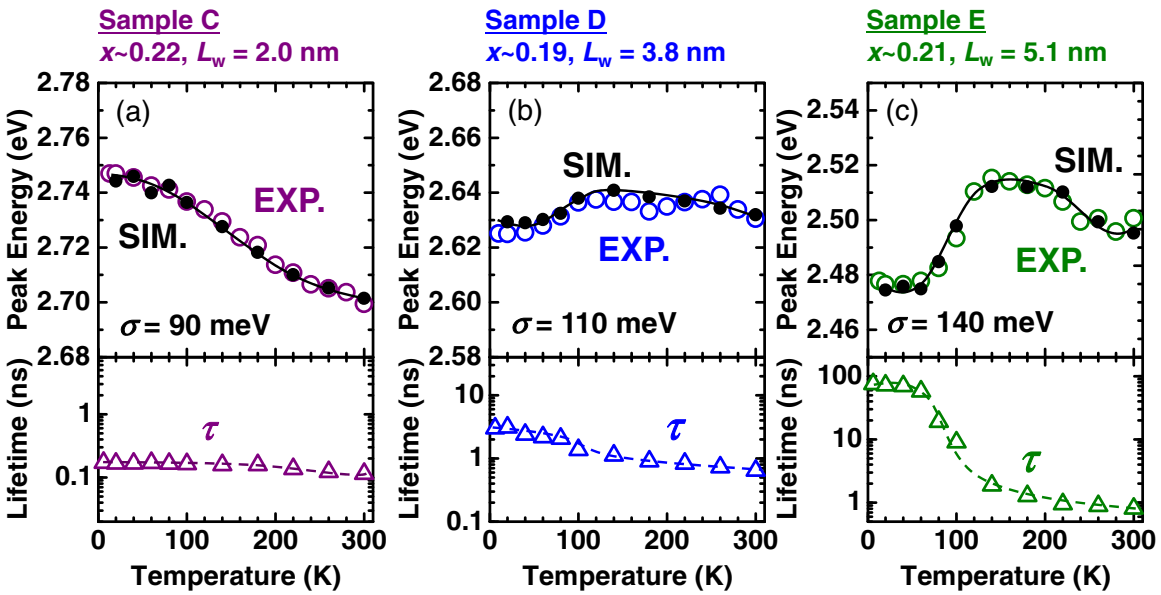

FIG. 10. PL peak energies (upper) and recombination lifetimes (lower) of samples (a) C ($x = 0.22$, $L_w = 2.0$ nm), (b) D ($x = 0.19$, $L_w = 3.8$ nm), and (c) E ($x = 0.21$, $L_w = 5.1$ nm). Filled circles represent the simulation results calculated by the method developed in this paper. The fitted σ values are 90, 110, and 140 meV for samples C, D, and E, respectively. Solid and dashed lines are included as a visual guide.

TABLE III. Parameters obtained from the modified simulation.

Samples	σ (meV)	Γ (meV)	ν_0 (s^{-1})	$N\alpha^2$	E_0(0 K) (eV)	E_0(13 K) (eV) (PLE)	E_{CAL} (eV)
B	110	0	5×10^{12}	1	2.710	2.713	2.77
C	90	0	1×10^{13}	1	2.935		2.93
D	110	0	1×10^{12}	0.4	2.838		2.85
E	140	30	1×10^{12}	0.2	2.729		2.73

well, when a polarization-induced field exists [53]. On the other hand, other sources of fluctuation, such as well-width fluctuation [54] and statistically unavoidable alloy broadening [55] show the opposite dependence on well width. Therefore, the larger observed inhomogeneous broadening in the wider QWs can mainly be attributed to compositional fluctuations in In, even though the compositions of samples C to E are similar. Quantifying the contribution from each fluctuation may be a subject of a future study.

The estimated $N\alpha^2$ values were lower in the thicker QWs, suggesting that the lateral confinement of excitons was enhanced, likely due to the larger potential fluctuation in the thicker QWs. (The discussion on the influence of $N\alpha^2$ on the simulation can be found in Refs. [16,20].) The analysis of the dimension of localization using the TRPL results supported this argument. The detail of the analysis is given in Supplemental Material [50].

The lower ν_0 values calculated for the thicker QWs suggest a weaker hopping transfer probability in thicker QWs. We suspect that this may be related to the interaction between phonons and low-dimensionally confined excitons in the potential fluctuations, but further studies are necessary to clarify the origin.

To validate the estimated E_0(0 K) values, the transition energies were calculated using the Schrödinger equation for ideal $In_xGa_{1-x}N$/GaN SQWs, with the structural parameters used shown in Table I. Here, the internal electric field in the strained $In_xGa_{1-x}N$ on the $(11\bar{2}2)$ plane was taken into account, but free carriers were ignored. The excitonic transition energies E_{CAL} listed in Table III were calculated by subtracting the exciton binding energy from the calculated electron-hole transition energies (the exciton binding energy depends on QW structures and were calculated using the model in Ref. [56].) Despite the rough approximations, the calculated E_{CAL} values are in reasonable agreement with those deduced from the simulation, which confirms the effectiveness of our modified model.

The mechanism behind the temperature-induced blue-shift attributed to the reduction of the recombination lifetime is explained in Fig. 11, using data for sample E. Figure 11(a) shows the experimentally determined temperature dependence of the recombination lifetime: the lifetime decreases from ~75 ns at 5 K to 0.8 ns at RT. For further discussion, we selected lifetimes of 75, 10, 3, and 0.8 ns, which are indicated by the dashed lines. The temperature-induced peak energy variations for these lifetimes were simulated by the conventional method (i.e., using constant lifetimes), with the other parameters used being the same as those in Table III, the results of which are shown in Fig. 11(b). The calculated peak energy for each lifetime monotonically shifts toward lower energies with increasing temperature. This is because, in this sample, the energy difference between sites is large with large inhomogeneous broadening ($\sigma = 140$ meV), which suppresses the thermal repopulation of excitons toward higher-energy states, even at RT. It must be noted that the shorter the lifetime, the higher the emission energy because shorter lifetimes prevent excitons from reaching deeper energy states. The calculated emission energy for a lifetime of 75 ns was 2.475 eV at a low temperature, as indicated by a' in Fig. 11(b); as the temperature increased up to ~140 K, the lifetime drastically decreased [a to d in Fig. 11(a)], and a blue-shift was observed in the emission energy [a' to d' in Fig. 11(b)]. Above 200 K, the lifetime was nearly constant at 0.8 ns [e and f in Fig. 11(a)], and the emission energy decreased as shown by points e' and f' in Fig. 11(b). In summary, in the temperature range where the lifetime steeply decreases, significant blue-shift is observed, demonstrating that the temperature dependence of the lifetime can account for the PL blue-shift.

Figure 12 illustrates a schematic for the mechanism behind the blue-shift, in which it is considered to be driven by the reduction of the exciton lifetime. At low temperatures, photogenerated excitons hop toward lower-energy states via phonon-assisted tunneling, where they are localized and radiatively recombine with the lifetime τ_{rad}. At elevated temperatures, there are two possible scenarios: first, if the lifetime does not significantly change, the hopping distance increases and, thus, excitons transfer to the lower-energy regions, which results in the red-shift of the peak energies

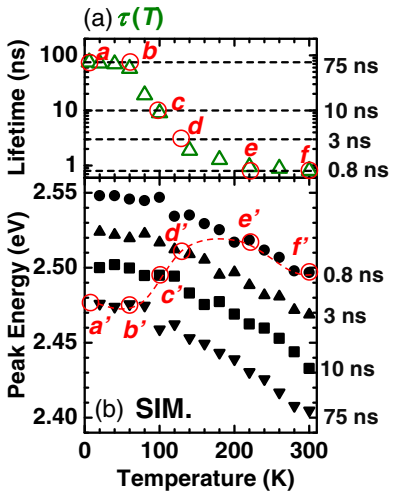

FIG. 11. (a) The recombination lifetime of sample E ($x = 0.21$, $L_w = 5.1$ nm) as a function of temperature. Horizontal dashed lines are designated for $\tau_0 = 75$, 10, 3, or 0.8. (b) Peak energies simulated by the conventional method with $\tau_0 = 75$, 10, 3, and 0.8 ns as functions of temperature. Points $a-f$ in (a) correspond to the points $a'-f'$ in (b).

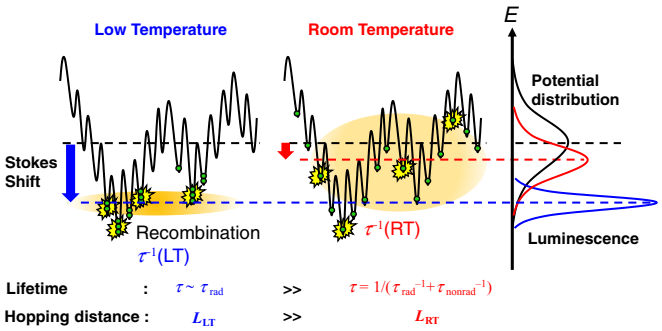

FIG. 12. Schematic diagram of exciton hopping dynamics in a disordered potential at low temperature and RT, in which the recombination lifetime decreases with increasing temperature. L denotes the hopping distance.

(larger Stokes shift). This is the case for sample C, shown in Fig. 10(a). On the other hand, sample E is representative of the second case where the lifetime drastically decreases, and excitons cannot reach deeper energy states. Consequently, recombining excitons are able to distribute in a higher-energy region than those at lower temperatures, which results in the observed blue-shift of the luminescence peak energies (smaller Stokes shift). It is deduced that the degree of the peak shift is strongly affected by the degrees of the lifetime variation and potential fluctuation, which is discussed in more detail in the next section.

VI. TWO DIFFERENT ORIGINS OF BLUE-SHIFTS

At an elevated temperature, hopping suppressed by a shortened lifetime and that enhanced via Eq. (2) compete with each other to determine the temperature-induced peak shift. The model developed in this study considers both factors, while the conventional constant lifetime model [8,10] considers only the latter factor. In the previous section, we demonstrated that the various temperature-induced peak shifts in the semipolar $(11\bar{2}2)$ SQW samples cannot be explained without considering the temperature-related lifetime variations. From this study, one question that arises is when the conventional constant lifetime model [8,10] is applicable, and when the model developed in this study should be used. To answer this question, we performed the same analyses as used in Sec. V for the polar sample and sample A ($x = 0.14$, $L_w = 4.0$ nm), which were well reproduced by the conventional model presented in Figs. 4(a) and 4(b). Figure 13 shows the temperature dependence of the PL peak energies and lifetimes of those samples; also shown are the simulation results derived from the model developed in this study. Even though the parameters used were the same as those for the conventional model (Table II), the model in this study proved to be equally suitable for reproducing the experimental results. Therefore, at this stage, we can conclude that the temperature-induced blue-shifts in these two samples can be attributed to (i) thermally activated repopulation of excitons at higher-energy states, and/or (ii) exciton recombination before

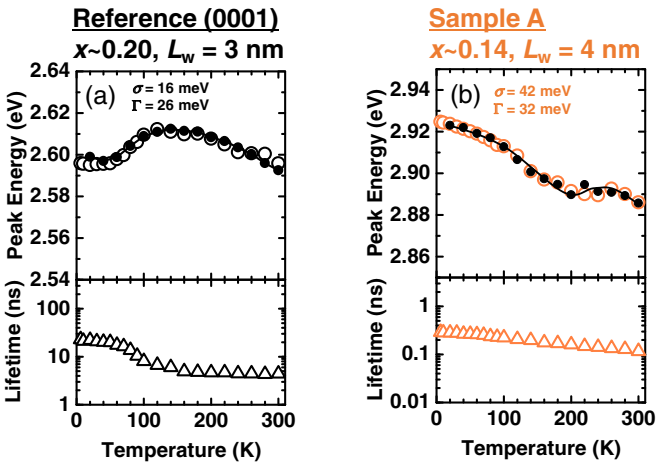

FIG. 13. Fitting to the PL peak energies of (a) the polar sample and (b) sample A ($x = 0.14$, $L_w = 4.0$ nm), using the model developed in this study. Open and filled symbols represent the experimental and simulated data, respectively. The experimentally determined $\tau(T)$ values are shown in lower panels.

relaxation to deeper energy states due to the shortening of lifetimes with increasing temperature.

To clarify which of these factors contributes more strongly to the peak shift, we investigate the correlation between the recombination lifetime and the exciton population in the distributed potential. Figure 14 shows the experimentally evaluated recombination lifetimes and Stokes shifts of the semipolar $(11\bar{2}2)$ and polar (0001) SQWs as functions of temperature. To compare different samples, dimensionless parameters such

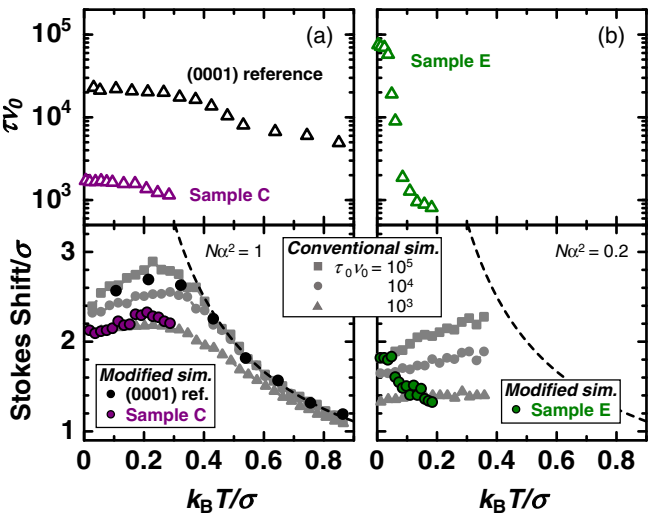

FIG. 14. Recombination lifetimes and Stokes shifts of semipolar $(11\bar{2}2)$ and polar (0001) SQWs as functions of temperature. Panel (a) is for the (0001) reference QW and sample C with $N\alpha^2 = 1$, and (b) is for sample E with $N\alpha^2 = 0.2$. For the $N\alpha^2$ values, see Tables II and III. Dimensionless physical parameters are used. Gray symbols in the lower panel are simulation results obtained by the conventional method with $\tau_0\nu_0 = 10^i$ ($i = 3$ to 5). The dashed line was analytically calculated with $\Delta E_{\mathrm{Stokes}}(T) = \sigma^2/k_BT$.

as $\tau\nu_0$, $\Delta E_{\mathrm{Stokes}}/\sigma$, and $k_{\mathrm{B}}T/\sigma$ were used, where the ν_0 and σ values were taken from Table III. In the lower panels of Figs. 14(a) and 14(b), the dashed lines are the analytically calculated Stokes shift, $\Delta E_{\mathrm{Stokes}}(T) = \sigma^2/k_{\mathrm{B}}T$. These curves assume infinite τ, are insensitive with $\tau_0\nu_0$ values, and express the blue-shift of emission peaks due to thermally equilibrium repopulation (which is referred to as *thermalization limit*). In this regime, thermally activated exciton hopping determines the peak shift. In addition, the Stokes shifts simulated by the conventional method are also plotted in the same panel with gray symbols, where the $\tau_0\nu_0$ values are 10^i ($i = 3$ to 5). The simulated Stokes shifts (gray symbols) show concave up characteristics. At higher $k_{\mathrm{B}}T/\sigma$ or with larger $\tau_0\nu_0$, the Stokes shift asymptotically approaches the analytical curve, i.e., the thermalization limit. On the other hand, at lower $k_{\mathrm{B}}T/\sigma$ or with smaller $\tau_0\nu_0$, the Stokes shift departs from the thermalization limit and strongly depends on $\tau_0\nu_0$ values, where exciton localization and thermalization are in competition.

For the polar (0001) QW, the Stokes shifts deduced from the hopping simulation were quite close to the analytical curve at high temperatures, which indicates that the blue-shift is mainly determined by thermal repopulation processes. As such, the analytical expression $\sigma^2/k_{\mathrm{B}}T$ is applicable. In contrast, for semipolar $(11\bar{2}2)$ samples C and E, the large inhomogeneous broadening ($\sigma \sim 100$ meV) lowers $k_{\mathrm{B}}T/\sigma$, which prohibits the thermalization limit from being realized in the observed temperature range within the finite lifetime.

This can be understood by considering that significant inhomogeneity in the QWs prevents excitons from thermally repopulating in higher-energy states. As a result, the temperature dependencies of the peak energies strongly depend on the degree of the lifetime variation. The thinner $(11\bar{2}2)$ QW (sample C, $x = 0.22$, $L_{\mathrm{w}} = 2.0$ nm) does not exhibit a blue-shift because the lifetime is nearly independent of temperature, as shown in Fig. 14(a). On the other hand, the thicker $(11\bar{2}2)$ QW (sample E, $x = 0.21$, $L_{\mathrm{w}} = 5.1$ nm) shows a blue-shift due to the steep reduction of the lifetime.

These considerations indicate that there are at least two mechanisms responsible for the luminescence blue-shift. In largely inhomogeneous systems, such as our thicker $(11\bar{2}2)$ QWs, the decrease of the recombination lifetime with increasing temperature causes the blue-shift. In a relatively homogeneous system, like the polar (0001) QWs, thermal repopulation of excitons (due to enhanced hopping) mainly causes the blue-shift, when the conventional constant lifetime model can well approximate experimental observations, as has been reported in many previous studies [8,10,11].

We observed the larger short-range inhomogeneity σ and smaller long-range inhomogeneity Γ in semipolar $(11\bar{2}2)$ QWs than in the polar (0001) QWs, despite the similarity between the two QW structures (for example, compare the semipolar sample D with the polar sample, both of which have an In composition of ~20% and a well width of ~3 nm). Nanoscopic optical properties can be different between polar (0001) and semipolar $(11\bar{2}2)$ QWs; in fact, while a SNOM equipped with a fiber probe with a 30-nm aperture can resolve a broad (0001) PL spectrum into its individual components [29], but a 10-nm aperture is necessary to resolve a $(11\bar{2}2)$ PL spectrum [57]. In addition, with an optical microscope, which has a much worse resolution than SNOM, the $(11\bar{2}2)$ QWs exhibit quite uniform emission patterns [41,57], which indicate the absence of long-range fluctuations, and evidence for $\Gamma = 0$, as revealed in this study. More detailed studies in this area are currently in progress.

Finally, the effect of the polarization field is discussed. Reference [22] claims that the energy dependence of the radiative recombination lifetime due to the polarization field plays a key role in the S-shaped peak shift, and the onset of the blue-shift is determined by the interplay between the energy-dependent radiative and energy-independent nonradiative recombination processes. This conclusion has been extracted from a comparison between polar and nonpolar $In_xGa_{1-x}N$ QWs; the former shows an S-shaped shift, but the latter does not. On the other hand, our model indicates that an S-shaped peak shift can happen even without the energy dependence of the radiative recombination process. (In other words, we can say that S-shaped peak shifts can be absent even with the energy dependence of the radiative recombination process.) Figure 4 indicates that although the electric field is stronger in sample B than sample A due to the higher In composition, the S-shaped peak shift is visible in sample A but invisible in sample B, contrary to an expectation from Ref. [22]. Additionally, Figs. 9 and 10 indicate that samples C, D, and E exhibit the considerably different peak shifts, in spite of similar electric fields. Therefore, we consider that although the electric field indeed exists in our samples, it plays a minor role in determining the PL peak shift, and the temperature dependence of the recombination lifetime is more crucial. The discussion in the Supplemental Material [50] also supports this consideration. For nonpolar QWs, our model also predicts monotonous red-shift due to the following reasons. The PL linewidth of the nonpolar QW in Ref. [22] is broad (200–300 meV), suggesting a large σ. In addition, the PL lifetime variation due to temperature is presumably small because the radiative recombination lifetime is intrinsically short due to the absence of the electric field. These situations are quite similar to those in our sample C, which cannot reach the thermalization limit due to the large σ as shown in Fig. 14(a), and shows the monotonous peak shift (Fig. 10). At present, both Ref. [22] and our model can explain the observation, and further study seems necessary for nonpolar QWs.

VII. CONCLUSIONS

Various temperature dependencies of the PL peak energies and FWHMs in $In_xGa_{1-x}N$/GaN SQWs grown on semipolar $(11\bar{2}2)$ GaN bulk substrates were analyzed. The experimental results could not be reproduced using a conventional exciton hopping model that assumes that recombination lifetimes are temperature independent. Therefore, we developed a method that takes into consideration the temperature-dependent recombination lifetime. This method quantitatively explains the experimental PL properties of the semipolar $(11\bar{2}2)$ and polar (0001) QWs quite well. Detailed analyses indicated that the PL blue-shifts can be caused not only by the exciton thermal repopulation, which is often reported for (0001) QWs, but also by the temperature-induced decrease of the

recombination lifetime. Particularly for material systems with large inhomogeneity and large lifetime variations, the latter effect can play a more significant role. The model developed in this study takes both mechanisms into account, and we believe that it can be universally applied to other disordered systems.

ACKNOWLEDGMENTS

This work is partially supported by JSPS KAKENHI Grants No. JP15H05732, No. JP16H02332, and No. JP16H06426, and by MEXT C-PhoST program. The authors would like to acknowledge Dr. M. Ueda and Dr. J. Nishinaka for their stimulated discussion and support with the MOVPE growth.

[1] T. Mukai, M. Yamada, and S. Nakamura, Jpn. J. Appl. Phys. **38**, 3976 (1999).
[2] A. Khan, K. Balakrishnan, and T. Katona, Nat. Photonics **2**, 77 (2008).
[3] S. Nakamura and G. Fasol, *Blue Laser Diode*, 2nd ed. (Springer, Heidelberg, 2000).
[4] Y. Enya, Y. Yoshizumi, T. Kyono, K. Akita, M. Ueno, M. Adachi, T. Sumitomo, S. Tokuyama, T. Ikegami, K. Katayama, and T. Nakamura, Appl. Phys. Express **2**, 082101 (2009).
[5] O. Jani, I. Ferguson, C. Honsberg, and S. Kurtz, Appl. Phys. Lett. **91**, 132117 (2007).
[6] S. Chichibu, T. Azuhata, T. Sota, and S. Nakamura, Appl. Phys. Lett. **69**, 4188 (1996).
[7] Y. Narukawa, Y. Kawakami, S. Fujita, S. Fujita, and S. Nakamura, Phys. Rev. B **55**, R1938(R) (1997).
[8] P. G. Eliseev, P. Perlin, J. Lee, and M. Osiski, Appl. Phys. Lett. **71**, 569 (1997).
[9] Y. H. Cho, G. H. Gainer, A. J. Fischer, J. J. Song, S. Keller, U. K. Mishra, and S. P. DenBaars, Appl. Phys. Lett. **73**, 1370 (1998).
[10] K. Kazlauskas, G. Tamulaitis, P. Pobedinskas, A. Žukauskas, M. Springis, C.-F. Huang, Y.-C. Cheng, and C. C. Yang, Phys. Rev. B **71**, 085306 (2005).
[11] M. Funato, Y. S. Kim, T. Hira, A. Kaneta, Y. Kawakami, T. Miyoshi, and S. Nagahama, Appl. Phys. Express **6**, 111002 (2013).
[12] Y.-H. Cho, G. H. Gainer, J. B. Lam, J. J. Song, W. Yang, and W. Jhe, Phys. Rev. B **61**, 7203 (2000).
[13] K. Kazlauskas, A. Žukauskas, G. Tamulaitis, J. Mickevičius, M. S. Shur, R. S. Q. Fareed, J. P. Zhang, and R. Gaska, Appl. Phys. Lett. **87**, 172102 (2005).
[14] H. Murotani, Y. Yamada, T. Taguchi, R. Kato, and T. Yokogawa, Phys. Status Solidi C **7**, 1884 (2010).
[15] M. Silver, G. Schoenherr, and H. Baessler, Phys. Rev. Lett. **48**, 352 (1982).
[16] S. D. Baranovskii, R. Eichmann, and P. Thomas, Phys. Rev. B **58**, 13081 (1998).
[17] K. Kazlauskas, G. Tamulaitis, A. Žukauskas, M. A. Khan, and J. W. Yang, Appl. Phys. Lett. **83**, 3722 (2003).
[18] C. Karcher, K. Jandieri, B. Kunert, R. Fritz, M. Zimprich, K. Volz, W. Stolz, F. Gebhard, S. D. Baranovskii, and W. Heimbrodt, Phys. Rev. B **82**, 245309 (2010).
[19] O. Rubel, S. D. Baranovskii, K. Hantke, B. Kunert, W. W. Ruhle, P. Thomas, K. Volz, and W. Stolz, Phys. Rev. B **73**, 233201 (2006).
[20] B. DalDon, K. Kohary, E. Tsitsishvili, H. Kalt, S. D. Baranovskii, and P. Thomas, Phys. Rev. B **69**, 045318 (2004).
[21] T. Makino, K. Saito, A. Ohtomo, M. Kawasaki, R. T. Senger, and K. K. Bajaj, J. Appl. Phys. **99**, 066108 (2006).
[22] T. Langer, H.-G. Pietscher, F. A. Ketzer, H. Jönen, H. Bremers, U. Rossow, D. Menzel, and A. Hangleiter, Phys. Rev. B **90**, 205302 (2014).
[23] Y. Narukawa, Y. Kawakami, S. Fujita, and S. Nakamura, Phys. Rev. B **59**, 10283 (1999).
[24] B. Monemar, Phys. Rev. B **10**, 676 (1974).
[25] H. Kalt, J. Collet, S. D. Baranovskii, R. Saleh, P. Thomas, L. S. Dang, and J. Cibert, Phys. Rev. B **45**, 4253 (1992).
[26] A. Miller and E. Abrahams, Phys. Rev. **120**, 745 (1960).
[27] Y. Kawakami, K. Nishizuka, D. Yamada, A. Kaneta, M. Funato, Y. Narukawa, and T. Mukai, Appl. Phys. Lett. **90**, 261912 (2007).
[28] A. Kaneta, Y.-S. Kim, M. Funato, Y. Kawakami, Y. Enya, T. Kyono, M. Ueno, and T. Nakamura, Appl. Phys. Express **5**, 102104 (2012).
[29] A. Kaneta, K. Okamoto, Y. Kawakami, and S. Fujita, Appl. Phys. Lett. **81**, 4353 (2002).
[30] V. Liuolia, A. Pinos, S. Marcinkeviius, Y. D. Lin, and H. Ohta, Appl. Phys. Lett. **97**, 151106 (2010).
[31] Y. Iwata, T. Oto, D. Gachet, R. G. Banal, M. Funato, and Y. Kawakami, J. Appl. Phys. **117**, 115702 (2015).
[32] S. Rudin, T. L. Reinecke, and B. Segall, Phys. Rev. B **42**, 11218 (1990).
[33] V. Y. Davydov, Y. E. Kitaev, I. N. Goncharuk, A. N. Smirnov, J. Graul, O. Semchinova, D. Uffmann, M. B. Smirnov, A. P. Mirgorodsky, and R. A. Evarestov, Phys. Rev. B **58**, 12899 (1998).
[34] A. Kasic, M. Schubert, Y. Saito, Y. Nanishi, and G. Wagner, Phys. Rev. B **65**, 115206 (2002).
[35] A. J. Fischer, W. Shan, G. H. Park, J. J. Song, D. S. Kim, D. S. Yee, R. Horning, and B. Goldenberg, Phys. Rev. B **56**, 1077 (1997).
[36] P. Lautenschlager, M. Garriga, S. Logothetidis, and M. Cardona, Phys. Rev. B **35**, 9174 (1987).
[37] M. O. Manasreh, Phys. Rev. B **53**, 16425 (1996).
[38] Y. S. Huang, Fred H. Pollak, S. S. Park, K. Y. Lee, and H. Morkoç, J. Appl. Phys. **94**, 899 (2003).
[39] K. P. Korona, A. Wysmołek, K. Pakuła, R. Stępniewski, J. M. Baranowski, I. Grzegory, B. Łucznik, M. Wróblewski, and S. Porowski, Appl. Phys. Lett. **69**, 788 (1996).
[40] Q. Guo and A. Yoshida, Jpn. J. Phys. Lett. **33**, 2453 (1994).
[41] J. Nishinaka, M. Funato, and Y. Kawakami, Appl. Phys. Lett. **106**, 082105 (2015).
[42] M. Funato, D. Inoue, M. Ueda, Y. Kawakami, Y. Narukawa, and T. Mukai, J. Appl. Phys. **107**, 123501 (2010).
[43] R. W. Martin, P. G. Middleton, K. P. O'Donnell, and W. Van der Stricht, Appl. Phys. Lett. **74**, 263 (1999).
[44] J. Feldmann, G. Peter, E. O. Göbel, P. Dawson, K. Moore, C. Foxon, and R. J. Elliott, Phys. Rev. Lett. **59**, 2337 (1987).
[45] C. H. Henry and D. V. Lang, Phys. Rev. B **15**, 989 (1977).

[46] T. Izumi, Y. Narukawa, K. Okamoto, Y. Kawakami, Sg. Fujita, and S. Nakamura, J. Lumin. **87–89**, 1196 (2000).
[47] R. Aleksiejūnas, K. Gelžinytė, S. Nargelas, K. Jarašiūnas, M. Vengris, E. A. Armour, D. P. Byrnes, R. A. Arif, S. M. Lee, and G. D. Papasouliotis, Appl. Phys. Lett. **104**, 022114 (2014).
[48] C. Gourdon and P. Lavallard, Phys. Status Solidi B **153**, 641 (1989).
[49] M. Gurioli, A. Vinattieri, M. Colocci, C. Deparis, J. Massies, G. Neu, A. Bosacchi, and S. Franchi, Phys. Rev. B **44**, 3115 (1991).
[50] See Supplemental Material at http://link.aps.org/supplemental/10.1103/PhysRevB.96.125305 for the fundamental PL properties of Samples C, D, and E, and supporting analyses for the $N\alpha^2$ estimates.
[51] S. L. Chuang and C. S. Chang, Phys. Rev. B **54**, 2491 (1996).
[52] A. Sasaki, K. Nishizuka, T. Wang, S. Sakai, A. Kaneta, Y. Kawakami, and S. Fujita, Solid State Commun. **129**, 31 (2004).
[53] C. Bodin, R. André, J. Cibert, L. S. Dang, D. Bellet, G. Feuillet, and P. H. Jouneau, Phys. Rev. B **51**, 13181 (1995).
[54] K. C. Zeng, M. Smith, J. Y. Lin, and H. X. Jiang, Appl. Phys. Lett. **73**, 1724 (1998).
[55] E. F. Schubert, E. O. Göbel, Y. Horikoshi, K. Ploog, and H. J. Queisser, Phys. Rev. B **30**, 813 (1984).
[56] M. Funato and Y. Kawakami, J. Appl. Phys. **103**, 093501 (2008).
[57] M. Funato and Y. Kawakami, Proc. SPIE **9363**, 93631T (2015).